



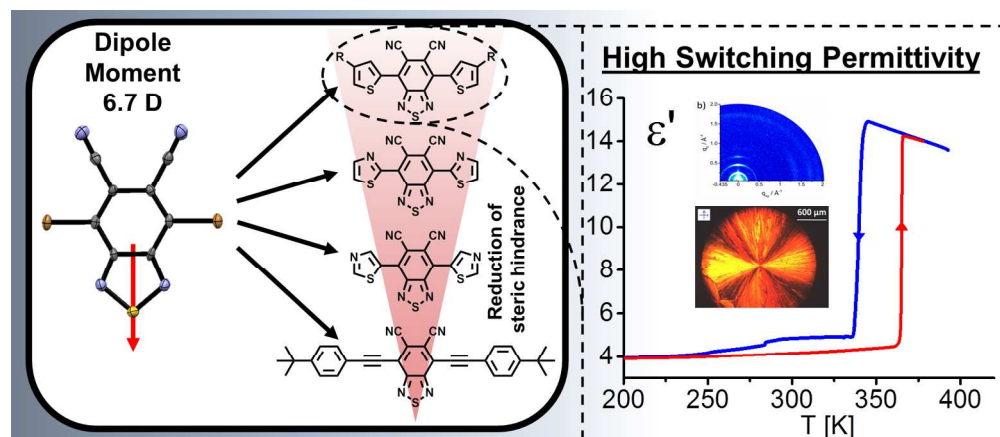
This document is the Accepted Manuscript version of a Published Work that appeared in final form in ACS Applied Materials and Interfaces

To access the final edited and published work see  
<https://pubs.acs.org/doi/10.1021/acsami.7b03060>

Wudarczyk, J., Papamokos, G., Marszalek, T., Nevolianis, T., Schollmeyer, D., Pisula, W., et al. (2017). Dicyanobenzothiadiazole Derivatives Possessing Switchable Dielectric Permittivities. ACS Applied Materials and Interfaces, 9(24), 20527-20535. doi:10.1021/acsami.7b03060.

# Dicyanobenzothiadiazole Derivatives Possessing Switchable Dielectric Permittivities

Wudarczyk, J., Papamokos, G., Marszalek, T.,  
Nevolianis, T., Schollmeyer, D., Pisula, W., et al.



TOC graphic

335x144mm (150 x 150 DPI)

# Dicyanobenzothiadiazole Derivatives Possessing Switchable Dielectric Permittivities

Jakob Wudarczyk<sup>1</sup>, George Papamokos<sup>2</sup>, Tomasz Marszalek<sup>1</sup>, Thomas Nevolianis<sup>2</sup>, Dieter Schollmeyer<sup>3</sup>, Wojciech Pisula<sup>1,4</sup>, George Floudas<sup>2</sup>, Martin Baumgarten<sup>1</sup> and Klaus Müllen<sup>1\*</sup>

<sup>1</sup>Max Planck Institute for Polymer Research, Ackermannweg 10, D-55128, Mainz, Germany

<sup>2</sup>Department of Physics, University of Ioannina, 45110 Ioannina, Greece

<sup>3</sup>Institut für Organische Chemie, Johannes Gutenberg-Universität Mainz, 55128 Mainz, Germany

<sup>4</sup>Department of Molecular Physics, Faculty of Chemistry, Lodz University of Technology, Zeromskiego 116, 90-924 Lodz, Poland

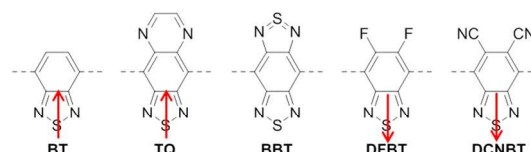
**ABSTRACT:** Benzothiadiazoles are important electron acceptors and are frequently employed as electron-deficient components of donor-acceptor polymers. We report the effect of nitrile-functionalities on the reactivity, steric hindrance, optoelectronic properties and dielectric permittivity in dicyanobenzothiadiazole (DCNBT). Dielectric spectroscopy in the bulk and in solution assisted by DFT-calculations revealed that these molecules can be engineered to engender maximum values of the dipole moment and of dielectric permittivity due to the strong electron-withdrawing effect of the nitrile groups. The self-assembly in the bulk was investigated by X-ray scattering performed on single crystals, fibers (2D-WAXS) and thin films (GiWAXS). Combining these results, we found a switching of dielectric permittivity of the 4,7-alkylthienyl-substituted dicyanobenzothiadiazole at the transition from the liquid crystalline to the isotropic phase with values capable of competing with the best known rod-like liquid crystals. **Keywords:** Donor-Acceptor-Compounds; Dielectric Permittivity; Benzothiadiazole; DCNBT; Thiadiazole; Dipole Moment;

The dipolar properties of low band gap materials play a fundamental role in the process of charge generation and charge separation. For example, pushing the limits of organic photovoltaics relates to methods of increasing dielectric permittivity.<sup>1</sup> The latter depends on the number density of dipoles, their values, and the orientation correlations between them. However, the dielectric permittivity of most organic materials is low and Coulombic attraction between electron-hole pairs (e.g. excitons) can lead to significant recombination losses that limit the power conversion efficiency. The exciton binding energy is:

$$E_b = \frac{e^2}{4\pi\epsilon_0\epsilon r} \quad (1)$$

where  $e$  is the elementary charge,  $\epsilon_0$  is the permittivity of free space,  $\epsilon$  is the dielectric permittivity of the medium and  $r$  the electron-hole separation. A way to circumvent these losses is by increasing the dielectric permittivity of the material that effectively increases Coulombic screening of charge carriers. Although low  $\epsilon$  values represent one of the most critical drawbacks in organic photovoltaics, only little attention<sup>2,3</sup> has been paid to engineer organic materials with high permittivities.

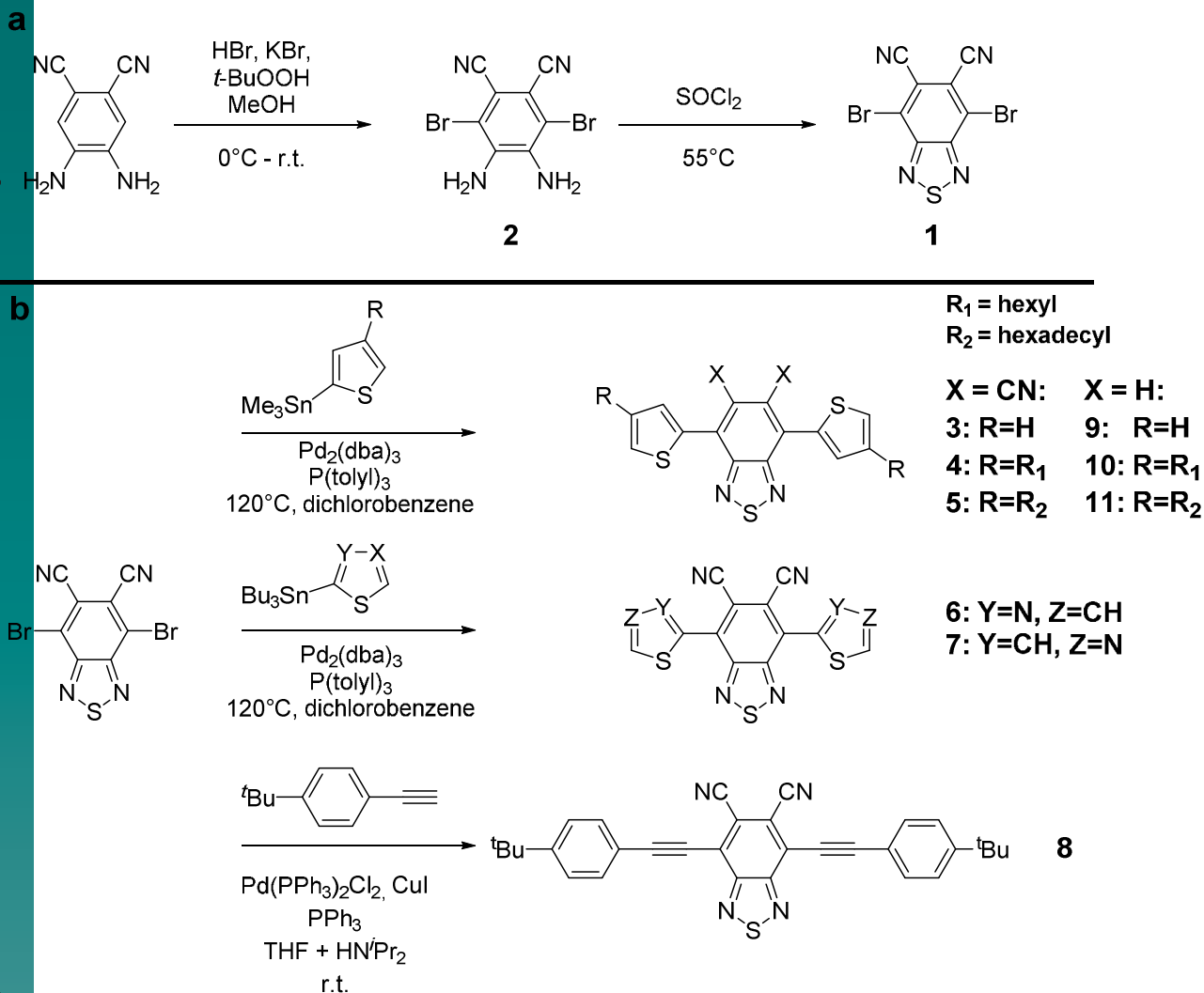
In organic electronics, conjugated donor-acceptor copolymers (D-A copolymers) have been the subject of intensive research over the last two decades resulting in materials that combine low bandgap<sup>4-6</sup> with high charge carrier mobilities<sup>7-10</sup> and high open-circuit voltages<sup>11-13</sup> due to proper adjustment of molecular orbitals in fullerene-based bulk-heterojunction solar cells. The present work targets donor-acceptor materials that combine high dielectric permittivities with low LUMO energies via incorporation of a highly dipolar



Dipole Moment	1.9 D	1.3 D	0 D	0.7 D	6.2 D
E(HOMO) / eV	-6.93	-6.70	-6.52	-6.95	-8.02
E(LUMO) / eV	-2.66	-3.50	-3.79	-2.59	-3.89

Figure 1: Calculated E(HOMO) E(LUMO) energies (eV) and dipole moments (Debye) for molecules in vacuo at the DFT-B3LYP level of theory. Basis set: 6-31g\*\* for HOMO/LUMO calculations and aug-cc-pVTZ for dipole moments.

acceptor unit. In this context, within D-A copolymers, 4,7-dithieno-2,1,3-benzothiadiazole (**9**) represents a repeat unit of particular interest that allows for the fine tuning of optoelectronic properties by means of functionalization of the electron-deficient 2,1,3-benzothiadiazole (BT) in 5,6-positions.<sup>14</sup> The comparison of the different BT derivatives, presented in Figure 1, reveals that the compound that best combines the lowest LUMO with the highest dipole moment is 5,6-dicyano-benzothiadiazole (DCNBT). Thus, synthetic chemists have faced the challenge to synthesize a 4,7-functionalized DCNBT unit facilitating cross-coupling reactions. 4,7-Dibromo-benzo[c][1,2,5]thiadiazole-5,6-dicarbonitrile (**1**) can be readily afforded from 4,5-diamino-3,6-dibromophthalonitrile (**2**). We recall here that a solution investigation by dielectric spectroscopy assisted by DFT calculations revealed that **2** possesses a record high dipole



Scheme 1: Synthetic procedures for (a) of 4,7-dibromobenzo[c][1,2,5]thiadiazole-5,6-dicarbonitrile (**1**) and (b) oligoarylenes for dielectric studies (**3-5**) and investigations of reduced steric hindrance (**6-8**).

moment. However, **2** cannot be directly employed in OPVs as it suffers from a high LUMO.<sup>15</sup>

With regards to photovoltaics it has to be mentioned that 4,7-thienyl-substituted BT-derivatives cannot be used in solar cells directly, but represent well-defined model compounds to illustrate differences in dipolar dynamics between highly dipolar and less dipolar compounds, since polymers containing them as repeat units have potential to provide excellent OPV-materials. Here, our study on is two-fold: First, we explore the effect of cyano substitution on the central BT unit (**4** vs. **10**). The introduction of variable dipole moments changes the energetics by an additional contribution reflecting dipole-dipole interaction energies that can further trigger self-assembly. Enhanced self-assembly is important for prospective processing of organic electronics, such as in inkjet printing.<sup>16</sup> Secondly, and in view of the importance of side chain engineering in solution processed organic electronics, we study the effect of alkyl side chain substitution (**4** vs. **5**). By combining dielectric spectroscopy with DFT calculations we show that these compounds can be engineered to have high dielectric permittivities and first molecular hyperpolar-

izabilities. We further explore the response of the dielectric properties to external stimuli, such as temperature, and show that the compounds have switching permittivities over a narrow temperature range. A switching permittivity at the phase transition from centrosymmetric crystalline (or liquid crystalline) to the isotropic phase gives insight into the properties of a field-induced oriented amorphous film (or matrix).

Heeney and co-workers, who prepared **3** through a less straight-forward route<sup>17</sup>, noticed steric hindrance of nitrile functions to adjacent thiophenes. The torsion of the thienyl-DCNBT bond leads to a deviation from the mean molecular plane (see crystal structure in Figure 2), which is consequently a disadvantageous factor for the indispensable  $\pi$ - $\pi$ -interaction in organic electronics<sup>18</sup>. Alternatively, arylenes like thiazoles have gained growing interest due to their ability to lower the energy of molecular orbitals<sup>19</sup> and increase crystallinity via interaction of the nitrogen lone pairs with e.g. antibonding orbitals of Sulphur atoms in adjacent thiophenes.<sup>20</sup> Thus, suitable derivatives have been synthesized and investigated with respect to steric hindrance between the DCNBT-unit and

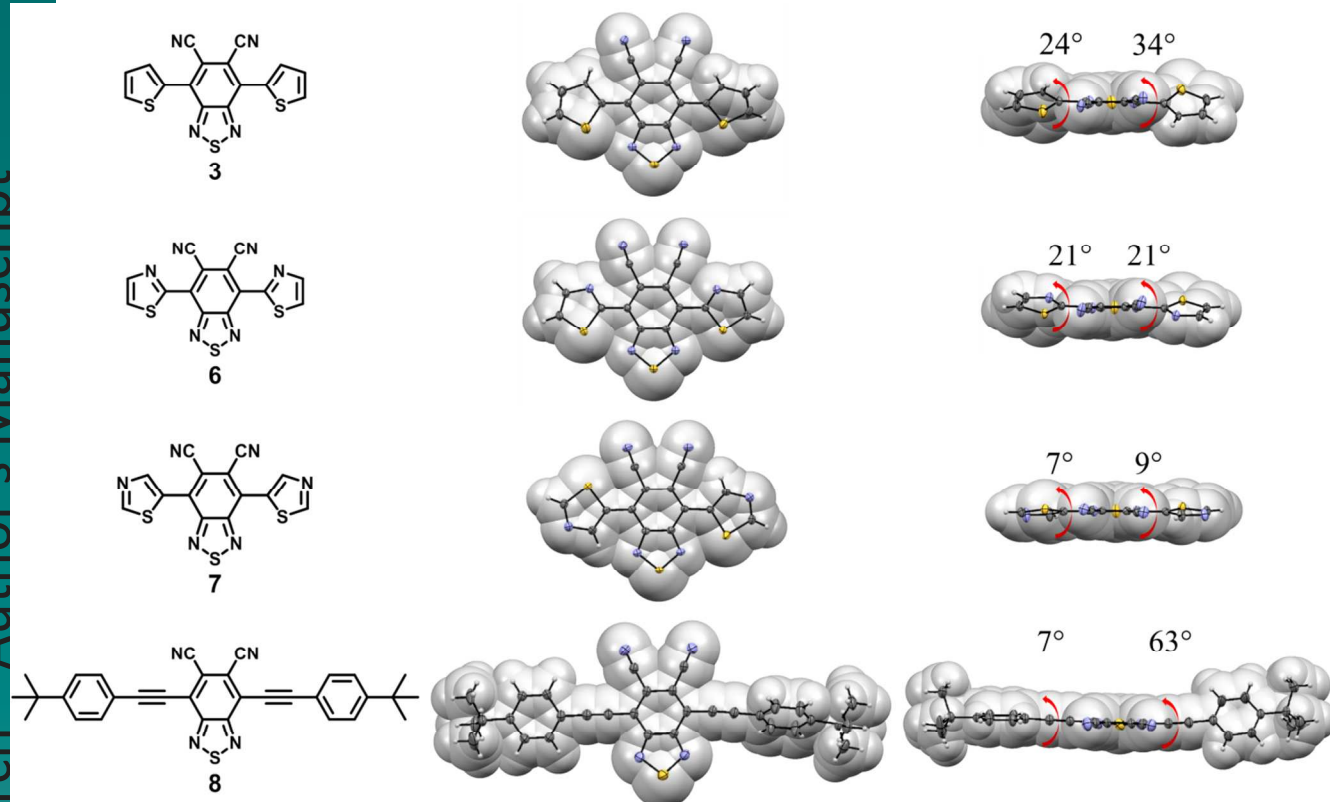


Figure 2: Crystal structures show successive reduction of steric hindrance of the cyano-groups attached to the central benzothiadiazole-unit with neighboring substituents. Torsional angles between aromatic units in compound **8** originate from packing in solid state (the crystal structures are illustrated as ORTEP drawings with thermal ellipsoids set at 50% probability overlaying spacefill-drawings to visualize the steric hindrance between neighboring aryl substituents).

It should be noted that the crystal structure has been measured at a different temperature previously (CCDC: 1020253).<sup>17</sup>

adjacent aryl-substituents via X-ray measurements made on single crystals. As the oligoarylenes **3**, **6-8** represent important model compounds for optoelectronic applications, the determination of electronic and photophysical properties was of significant importance.

## Synthesis

Parallel to our work<sup>15,21</sup>, several groups have recently synthesized functionalized 5,6-dicyanated benzothiadiazole<sup>17,22,23</sup>, benzotriazole<sup>23,24</sup> and quinoxaline.<sup>23</sup> Those approaches either hinge on already aryl-substituted precursors or optimized towards C-H-activated aryl-aryl-coupling. Our route however, represents a more convenient approach, since the brominated species **1** can undergo transition metal catalyzed coupling reactions under established<sup>25,26</sup> conditions.

Starting with 4,5-diamino-3,6-dibromophthalonitrile (**2**), ring-closure with thionyl chloride facilitated **1** after 30 h at 55°C (Scheme 1). We found that longer reaction times and higher temperatures caused nucleophilic substitution of bromine by chloride. Furthermore, we were able to increase the yield of 52% to 80% via distillation of the remaining thionyl chloride under reduced pressure, instead of work-up with cooled potassium carbonate solution. The 4,7-dibromobenzo-*c*[[1,2,5]thiadiazole-5,6-dicarbonitrile (**1**) can undergo transition-metal catalyzed cross-coupling with tin compounds via Stille reaction. Here we found that using Pd<sub>2</sub>(dba)<sub>3</sub> instead of Pd(PPh<sub>3</sub>)<sub>4</sub> catalyst resulted in higher yields. Thus, we were

able to increase the yield from 25% to 65%. The non-cyanated derivatives 4,7-bis(4-hexylthiophen-2-yl)benzo-*c*[[1,2,5]thiadiazole (**10**) and 4,7-bis(4-hexadecylthiophen-2-yl)benzo-*c*[[1,2,5]thiadiazole (**11**) have been synthesized by the same procedure in yields of 60% and 82% respectively.

Figure 2 shows the crystal structures of several model compounds. Whereas a steric hindrance in **3** noted by Heeney<sup>17</sup> and to a similar extent in the trimethylsilylated derivative<sup>23</sup>, can be observed, a successive reduction of the displacement out of plane regarding the central DCNBT-unit is visible in **6-8**. Strikingly, the 2-thiazole-substituted molecule (**6**) suffer from a higher torsional (24°) angle than the 5-thiazole-analogue (**7**, 7° and 9° respectively), which reveals a higher steric hindrance of the cyano-groups and the nitrogen lone pair compared to the C-H-substituent. Comparison of **7** with **3**, on the other hand, shows a reduced torsion between thiazole and DCNBT. Furthermore, the different orientation of the two thiazoles in **6** suggests an almost vanished hindrance. However, due to the strong electron-withdrawing character of both coupling partners the yields of the thiazole-compounds were very low. The compound with the least steric hindrance, compound **8**, was obtained from a Sonogashira coupling reaction with 1-(*tert*-butyl)-4-ethynylbenzene in moderate yield of 47%. Although a torsional angle of 63° is observed here, this compound exposes the least steric hindrance and occurring torsion is based on packing effects in the solid state.

## Optoelectronic Properties

The synthesized oligoaryles **3** and **6-8** show strong fluorescence under black light illumination (see Figure 3), which encouraged us to investigate optoelectronic properties via determination by absorption spectroscopy, fluorescence spectroscopy, measurement of fluorescence quantum yields and cyclic voltammetry. Figure 4 shows the optical absorption spectra in the visible range and fluorescence of the model compounds **3**, **6**, **7** and **8**, while Table 1 summarizes their optical properties (detailed absorption spectra from 250-800 nm can be found in the supporting information). Generally, the extinction coefficients are roughly within the same range. In comparison with compound **3** all derivatives exhibit a hypsochromic shift of the absorption. Additionally, all compounds exhibit high quantum yields of 87% to 93%. Comparing the DCNBT-derivatives with non-cyanated derivatives (e.g. compound **9**: 72%<sup>27</sup>), an increasing effect on the quantum yield is exposed. Compound **8** reveals the highest quantum yield and the highest molar extinction coefficient. Remarkably, **8** is also the compound with the lowest Stokes shift in this row of model compounds. With the exception of **8** all compounds have a Stokes shift of about 120 nm. The lower shift in **8** is probably caused by lower vibrational loss from ground state to the excited state in solution, due to lower dihedral rotation-energy of ethynyl-substituents in this row of oligoaryles.

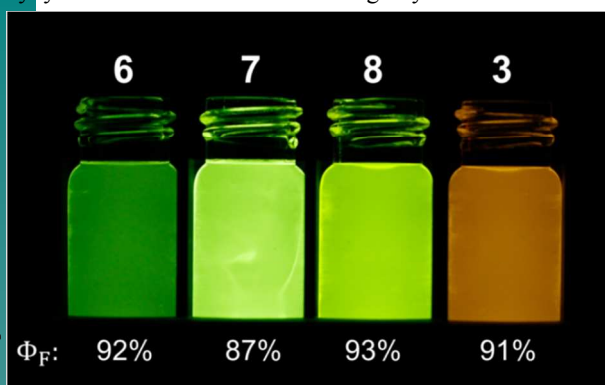


Figure 3: Photograph of compounds **3**, **6**, **7** and **8** under black light illumination with 365 nm.

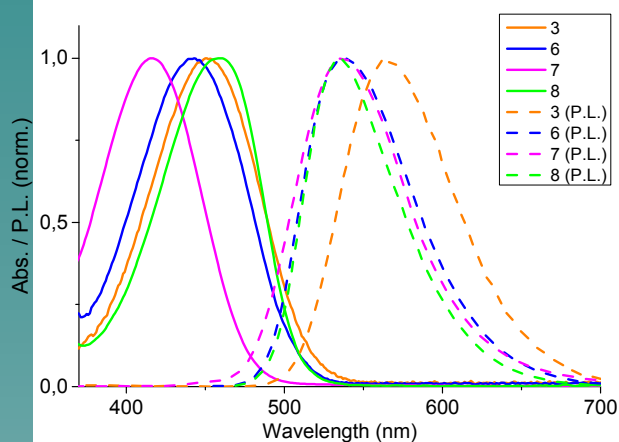


Figure 4: Normalized Absorption in the visible range and fluorescence spectra of model compounds **3**, **6**, **7** and **8**.

**Table 1: Photophysical properties obtained from absorption and fluorescence spectroscopy of model compounds **3**, **6**, **7** and **8** (detailed spectra of each compound can be found in the SI).**

Com pd.	$\lambda_{\max \text{ abs}}$ (nm)	$\lambda_{\text{onset}}$ (nm)	$\lambda_{\max \text{ em}}$ (nm)	Stokes shift (nm)	$\epsilon$ ( $\text{L M}^{-1} \text{cm}^{-1}$ )	$\Phi_F$
<b>3</b>	298, 446	517	565	119	$28.1 \times 10^3$	0.91
<b>6</b>	286, 416	485	539	123	$27.4 \times 10^3$	0.92
<b>7</b>	286, 416	484	538	124	$31.4 \times 10^3$	0.87
<b>8</b>	300, 458	509	536	78	$43.9 \times 10^3$	0.93

In general cyclic voltammetry (measured from solution using THF as solvent with concentrations of 1 mg/ml, see Table 2) revealed high electron affinities of the model compounds of 3.56 eV to 3.83 eV. Arylethynyl-substituents are weaker donors compared to thiophene but also allow different  $\pi$ - $\pi$  conjugation since the connecting carbon-atoms are sp-hybridized, which affects planarity, thus **8** compared to compound **3** has a higher electron affinity. Since the incorporation of more electronegative atoms causes a higher electron affinity, **6** and **7** show higher electron affinities than **3**, as expected.

## Computational results

The presented oligoarylenes contain a dipole moment in each arylene unit. Depending on their relative orientation, the overall molecular dipole moment, and consequently, the dielectric permittivity of the compound can be tuned. To assist the experimental studies on the dipolar dynamics and static dielectric permittivity, a theoretical treatment is employed for compounds **3** and **9** along with their alkylated derivatives **4**, **5**, **10** and **11**. (Computational method via a variety of appropriate functionals suitable for calculation of total molecular polarizability ( $\alpha$ ), first hyperpolarizability ( $\beta$ ) and HOMO-LUMO visualization for **3**, **4** and **5** results are given in S.I.; Table S2) The calculated dipole moments, are given in Table 3 (level of theory: DFT-CAM-B3LYP).

**Table 2: Calculated HOMO- and LUMO-energies and measured electron affinities by cyclic voltammetry**

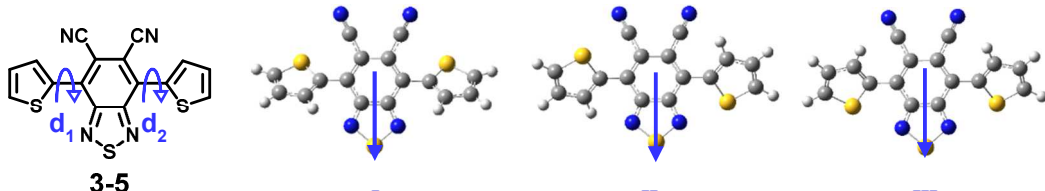
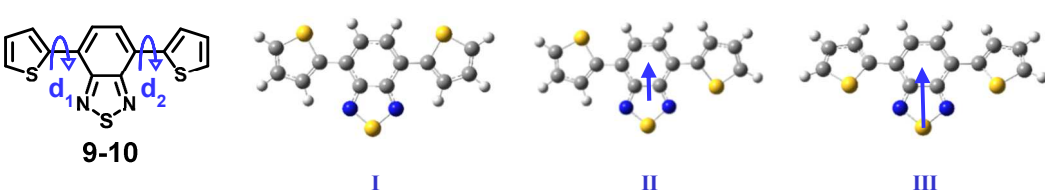
Compound	$E(\text{HOMO, calc}) / \text{eV}^a$	$E(\text{LUMO, calc}) / \text{eV}^a$	$\Delta E(\text{HOMO-LUMO}) / \text{eV}^a$	$E(0^-) / \text{V}^b$	$EA / \text{eV}^c$	$E_{\text{opt gap}} / \text{eV}^d$
<b>3</b>	-6.09	-3.39	2.70	-1.24	3.53	2.40
<b>6</b>	-6.41	-3.63	2.78	-0.97	3.83	2.56
<b>7</b>	-6.61	-3.69	2.92	-1.01	3.79	2.56
<b>8</b>	-5.59	-3.46	2.13	-1.13	3.69	2.44

<sup>a</sup>Level of theory: DFT, B3LYP, 6-31g\*. <sup>b</sup>First reduction potentials measured by cyclic voltammetry (CV) in THF with  $\text{Bu}_4\text{NPF}_6$  as the electrolyte against  $\text{Fc}/\text{Fc}^+$  as an internal standard (-4.80 eV) at 0.1 mV/s.

<sup>c</sup>Calculated from CV measurements [ $EA = -4.80 \text{ eV} - E(0^-)$ ]. <sup>d</sup>Calculated from the onset of the optical absorption.

Hyperpolarizabilities are of importance in the description of the nonlinear optical response of materials. Interestingly, the total molecular polarizability ( $\alpha$ ) is unaffected by conformational changes but its value is increasing upon addition of alkyl groups. On the other hand, as shown in Table 3, the molecular first hyperpolarizability ( $\beta$ ) is significantly affected

Table 3: Calculated dipole moments  $\mu_o$  (debye), total molecular polarizabilities  $\alpha$  ( $\times 10^{-40}$  C<sup>2</sup>m<sup>2</sup>J<sup>-1</sup>) and first hyperpolarizabilities  $\beta$  (debye-ang<sup>2</sup>) of **3**, **4**, **5** and **9**, **10**, **11** in various conformations. Level of theory: DFT-CAM-B3LYP. Basis set: for molecules **3** & **9** is aug-cc-pVDZ, for molecules **4** & **10** is 6-311++G(2d,2p) while for **5** & **11** is 6-31+(d,p). Blue arrows represent the vectors of dipole moment (not proportional to the calculated value). Arrows of dipole moments point to the positive end. The star (\*) instead, denotes that first hyperpolarizability values for molecules treated with the 6-31+G (d, p) basis set are not reported because this basis set expansion is not sufficient for the accurate prediction of this property. Atom color code: Blue=Cyan, Grey=Carbon, Yellow=Sulfur, White=Hydrogen.

				
		I	II	III
$\mu_o / \alpha / \beta$	<b>3</b>	7.2 / 47.4 / 206.7	6.6 / 47.7 / 209.8	6.0 / 48.0 / 213.6
	<b>4</b>	8.0 / 73.0 / 280.4	6.5 / 73.4 / 198.5	5.3 / 73.9 / 138.8
	<b>5</b>	8.0 / 111.2 / *	6.5 / 111.6 / *	5.2 / 115.1 / *
				
		I	II	III
$\mu_o / \alpha / \beta$	<b>9</b>	0.2 / 44.0 / 8.7	1.1 / 43.9 / 5.4	2.1 / 43.7 / 4.4
	<b>10</b>	0.7 / 70.2 / 39.3	0.7 / 70.5 / 63.0	2.9 / 69.7 / 12.8
	<b>11</b>	0.7 / 107.7 / *	0.7 / 108.4 / *	3.0 / 110.5 / *

both by the addition of alkyl groups and by conformational changes.

The theoretical treatment in vacuo of compounds **3-5** and **9-11** revealed several conformations with reference to the central thiadiazole unit (I: anti-anti, II: syn-anti III: syn-syn) resulting in various permanent dipole moments of the compounds (see Table 3 and Tables S3 and S4).

In general, the presence of the two cyano-groups in DCNBT induces a strong electron withdrawing effect and generates a reverse dipole moment vector with respect to that found in BT (see Figure 1). Evidently, molecules **3-5** can be tuned to engender maximum values of the dipole moment. The conformation that most ideally combines the highest dipole moment and first molecular hyperpolarizability is orientation I (Table 3 and S4). Subsequently, we employ compounds **4**, **5** and **10** possessing variable dipole moments (from 0.7 D to 8.0 D) and investigate their self-assembly and dynamics.

### Thermodynamics and self-assembly

The phase transformations in compounds **10** (possessing a weak dipole), **4** and **5** (both having stronger dipoles) can be discussed with respect to the DSC traces and POM images that provide, respectively, the crystallization/melting heats at the transition temperatures and the presence of superstructures. The POM textures of **4** and **5** are distinctly different from compound **10** suggesting crystalline (Cr) and liquid crystalline (LC) textures, respectively (Fig. S1). Furthermore, the POM image of **10** obtained under isothermal conditions (at 294 K)

displays a smectic liquid crystalline texture. This is in sharp contrast to the spherulitic textures obtained for **4** and **5**, typical of crystalline phases. In DSC, for **10**, two exothermic peaks are seen at 299 K and 305 K and three endothermic peaks at 318 K, 332 K and 336 K. In addition, for **4** and **5** two crystalline phases are evident in the cooling curve. The transition temperatures and corresponding heats are summarized in Table 4.

**4** crystallizes in a centrosymmetric structure with a P-1 space group, as observed by single crystal analysis (see Table S11). The crystal structure of **5** was investigated with wide-angle X-ray scattering from extruded fibers and the results are illustrated Figure 5. The figure depicts intensity contour plots as a function of temperature together with four representative 2D patterns. The 2D WAXS patterns and contour plots reveal a set of strong equatorial peaks indexed as (001) together with a set of meridional peaks. The meridional peaks at temperatures below 346 K, correspond to the (1 $\bar{2}$ 1), (021), (107), (20 $\bar{3}$ ) reflections from a triclinic unit cell with parameters  $a=0.82$  nm,  $b=0.985$  nm,  $c=2.86$  nm and  $\alpha=92.8^\circ$ ,  $\beta=95.14^\circ$ ,  $\gamma=110^\circ$  (called Cr<sub>B</sub>). At higher temperatures there is a transformation to another triclinic unit cell with parameters  $a=0.9$  nm,  $b=0.95$  nm,  $c=2.89$  nm and  $\alpha=92.8^\circ$ ,  $\beta=96.7^\circ$ ,  $\gamma=109.7^\circ$  (called Cr<sub>A</sub>). The phase transformation is evident in the intensity contour plot with the bifurcation of the (20 $\bar{3}$ ) reflection. Finally, the Cr<sub>A</sub> structure melts at 384 K (isotropic phase, I).

**Table 4: Transition temperatures and associated heats on cooling and subsequent heating (rate: 10 K/min).**

	Sample	Transition	Temp. / K	$\Delta H / \text{Jg}^{-1}$
Cooling	10	I→LC	299	62
	4	I→Cr	337	73
	5	I→Cr <sub>A</sub>	365	137
		Cr <sub>A</sub> →Cr <sub>B</sub>	-	-
Heating	10	LC→I	336	68
	4	Cr→I	368	80
	5	Cr <sub>B</sub> →Cr <sub>A</sub>	346	-
		Cr <sub>A</sub> →I	384	135

An identical Cr<sub>B</sub> crystal structure is found for spin-coated thin film of 5 by the analysis of the grazing incidence WAXS pattern in Figure S2b. The out-of-plane position of the (001) reflection is characteristic for an edge-on arrangement of the molecules, whereby the overall crystallinity is reduced in comparison to the extruded fiber sample. In contrast to 5, compound 4 shows higher order and a crystal structure which corresponds well to the unit cell determined in the single crystal analysis (Figure S2a, Table S12). Thereby, the molecules are also organized in an edge-on fashion on the substrate as evident from the in-plane  $\pi$ -stacking peak and the out-of-plane (001) reflection.

### Dielectric permittivity and dipolar dynamics

Experimental molecular dipole moments were evaluated both in solution and in the bulk state by dielectric spectroscopy (details in SI) at 25°C using a Novocontrol Alpha frequency analyzer (frequency range from  $10^{-2}$  to  $10^7$  Hz). Dilute solutions in THF (4, DCNBT and 1 due to low solubility in less polar solvents) and in chloroform (molecule 4) were prepared and the dielectric permittivity was measured as a function of solute concentration (Figure S4 and Table S1). Since both the solute and the solvent are polar we have employed the modified Onsager equation according to Böttcher<sup>28-30</sup>. Solution-based measurements generally showed high dipole moments of the cyanated compounds in the range of 6.1–7.7 debye, which is lower than the most polar benzenes<sup>15</sup> or quinones<sup>31</sup>, but as high as *p*-nitroaniline<sup>32</sup>. Whereas the slight decrease in dipole moment from  $7.7 \pm 0.4$  (DCNBT) to  $6.7 \pm 0.5$  (compound 1) is clearly attributed to the substitution of a proton by an electron-withdrawing bromo-substituent, the situation with molecule 4 is different. Here, measurements in two different polar solvents (THF and chloroform) revealed different dipole moments ( $7.6 \pm 0.2$  debye and  $6.1 \pm 0.3$  debye, respectively). This finding likely reflects different conformational preferences (anti-anti, anti-syn) of the molecule as predicted by DFT calculations (see Table 3).

In the bulk the dielectric permittivity is a sensitive probe of phase transformations. In addition, it contains information on the effective dipole moment (as compared to gas phase or solution dipole moment) of the compounds. Figure 6 shows the dielectric permittivity of 10, 4 and 5 under isochronal

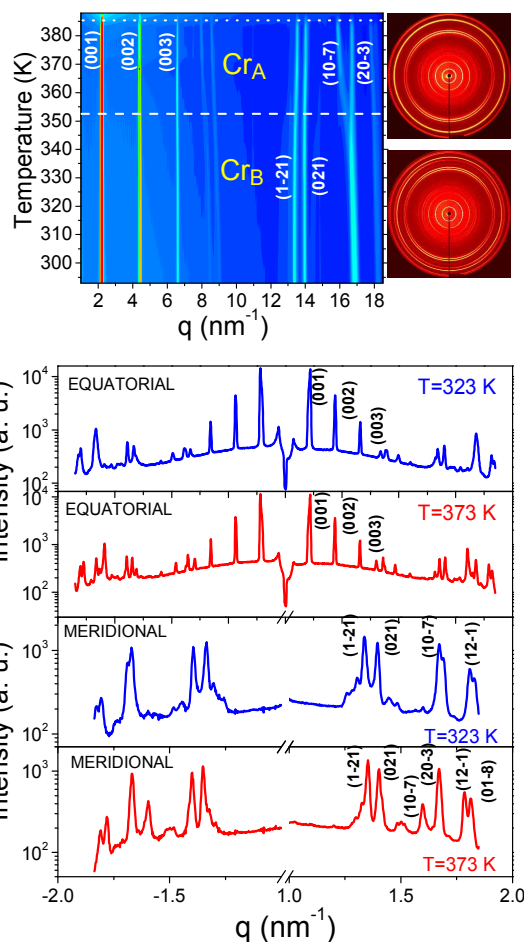


Figure 5: (Top-left) WAXS intensity contour plots corresponding to 5. The horizontal dashed line indicates the Cr<sub>B</sub> to Cr<sub>A</sub> phase transformation and the horizontal dotted line indicates the respective transition temperature from Cr<sub>A</sub> to the isotropic (I) phase. (001) peaks indicative of a lamellar arrangement. (Top-right) 2D-WAXS patterns obtained from extruded fibers at 323 K (top) and 373 K (bottom) during heating, corresponding to the Cr<sub>B</sub> and Cr<sub>A</sub> phases, respectively. (Bottom) Equatorial and meridional scattered intensity distributions in the 2D diffraction patterns at 323 K and 373 K. The scattered intensity maxima are assigned by the *hkl* indices of the corresponding lattices.

conditions obtained on cooling and subsequent heating. In all cases there is an abrupt reduction/increase in dielectric permittivity on cooling/heating through the crystalline-to-isotropic (in 4 and 5) or the LC-to-isotropic (in 10) transitions. The corresponding transition temperatures are very close to the ones obtained from DSC and reveal a pronounced hysteresis. At temperatures corresponding to the isotropic phase the dielectric permittivity scales as  $1/T$ . Kirkwood and later Fröhlich addressed the precise form of the static dielectric constant of polar liquids with short-range interactions between molecules. The theory has considered an infinite continuum of dielectric permittivity<sup>33,34</sup>,  $\epsilon_s'$ , and within this a spherical region containing  $N_0$  elementary dipoles that were treated explicitly. Based on these assumptions, the dielectric permittivity can be expressed as:



$$\varepsilon'_s = \varepsilon_\infty + \frac{1}{3\varepsilon_0} Fg \frac{\mu^2 N_0}{k_B T V} \quad (2)$$

Here,  $N_0/V$  is the number density of dipoles expressed as  $(\rho/M)N_A$ , where  $\rho$  is the mass density (defined above) and  $M$  is the molar mass,  $F = \varepsilon'_s(\varepsilon_\infty + 2)^2 / [2(\varepsilon'_s + \varepsilon_\infty)]$  is the local field,  $\mu$  is the dipole moment and  $g$  is the dipole orientation correlation function

$$g = 1 + \frac{\langle \sum_{i=1}^{N_0} \sum_{i < j} \mu_i \mu_j \rangle}{N_0 \mu^2} \quad (3)$$

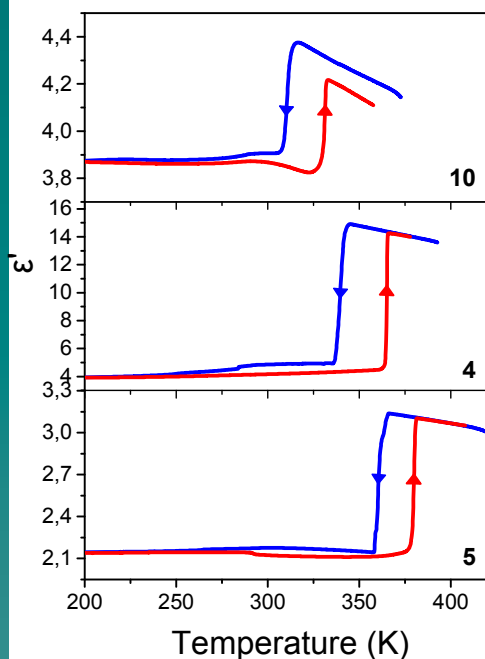


Figure 6: Dielectric permittivity of **10** (top), **4** (middle) and **5** (bottom) as a function of temperature under isochronal conditions (frequency of  $1.33 \times 10^5$  Hz) obtained with a cooling (blue) and heating (red) rates of 5 K/min. Note the large hysteresis in all compounds and the large switchable permittivity of compound **4**.

Considering only nearest neighbor orientation correlations, the above expression for the reference dipole surrounded by  $z$  equivalent nearest neighbors reduces to  $g = 1 + z \langle \cos \theta \rangle$ . Here,  $\theta$  is the angle between the reference dipole and one of its  $z$  nearest neighbors. We should keep in mind that what is measured in DS in the bulk is the effective dipole moment,  $\mu_{\text{eff}}^2 = g^* \mu_0^2$ , where  $\mu_0$  is the gas-phase dipole moment obtained from the simulations (Table 3). As we have shown in an earlier study on dipole-functionalized discotic liquid crystals<sup>35</sup>, the latter is sensitive to the actual packing (i.e., crystal structure in the solid state). The effective dipole moment measured in the bulk (by DS) can be very different from the solution or gas-phase dipole moments (DFT) and this is shown in Table 5. Here the effective dipole moment for the three compounds was calculated from the dielectric permittivity values and the dipole orientation correlation function through Eqs. 2 and 3. The effective dipole moments for the three compounds calculated through Eqs. 2 and 3 are shown in Table 5. For **10** there are two configurations that result in low dipole moments (0.7 and 0.8 for orientations I and II, respectively) as observed experi-

mentally ( $\mu_{\text{eff}} = 1.0$  D). Contrast this with compounds **4** and **5** where the experimental values of the effective dipole moment are substantially lower than the ones obtained from solution studies and simulations for all three orientations. As an example, for **4**, the resulting dipole orientation correlation function,  $g$ , assumes a value of 0.1, indicating that dipoles have preferred orientation correlations with large  $\theta$ 's. However, the most interesting feature of the permittivity curves in Fig. 6 is the large switchable permittivity of **4** within a narrow temperature range<sup>36-38</sup>. The change in  $\varepsilon'_s$  for **4** at the phase transition ( $\Delta\varepsilon \sim 11$ ) exceeds the one found in some semifluorinated azobenzene derivatives and is close to the well-known liquid crystal 5-CB ( $\Delta\varepsilon \sim 14$ )<sup>39</sup>. Because of their solid state packing, compounds with longer alkyl chains exhibit lower dielectric permittivity and are therefore less favorable with respect to the design of photoactive materials for bulk-heterojunction solar cells.

The dipolar dynamics within the different phases were investigated by frequency-dependent measurements under isothermal conditions. Of particular interest are the dynamics of **10** with the liquid crystalline order. The resulted dynamics are depicted in Figure 7 as a function of inverse temperature. Figure S3 gives representative loss curves of **10** at some selected temperatures. Different, partially overlapping processes are evident in the dielectric loss curves in addition to the conductivity contribution. The dynamics of rod-like liquid crystals in the nematic phase reflect different modes: the rotation of molecules about the short molecular axes gives rise to a slow process (called  $\delta$ ); the precession of long molecular axes about the director leads to a faster process (called  $\alpha$ ); the rotation about the long molecular axes is even faster. These dynamic features are distinct within the nematic phase because the nematic potential hinders rotation about the short axis. The intensity of the two modes varies as it depends on the orientation of the director with respect to the external electric field. For example, a director aligned parallel (perpendicular) to the electric field favors relaxation through the slower (faster)

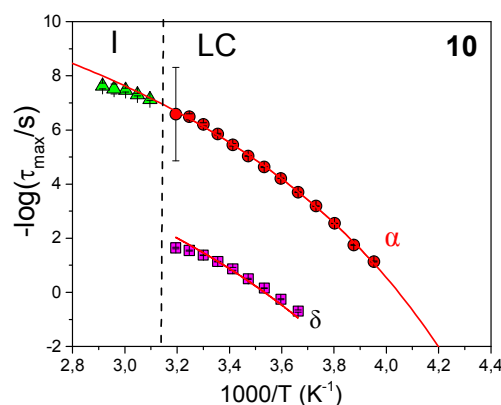


Figure 7: Temperature dependence of relaxation times for **10** in the usual Arrhenius representation. In the isotropic phase (I) there is a single process (triangles) that on cooling into the liquid crystalline phase (LC) gives rise to two relaxations: a fast  $\alpha$  process (spheres) and a slower  $\delta$  process (squares). Lines are fits to the VFT equation. The phase transition temperature is indicated by the vertical line.

process. Independent of the dielectric strength, the relaxation times,  $\tau(T)$ , both the  $\alpha$  process and the  $\delta$  process obey the Vogel-Fulcher-Tammann (VFT) equation,  $\tau = \tau_0 \exp(B/T-T_0)$ , where  $\tau_0$  is the relaxation time in the limit of very high temperatures,  $B$  is the activation parameter and  $T_0$  the “ideal” glass temperature located below the glass temperature  $T_g$ . The  $B$ ,  $T_0$  and  $T_g$  parameters assume values of  $2300 \pm 500$  K,  $176 \pm 10$  K and  $238 \pm 3$  K for the  $\delta$  and  $2300 \pm 400$  K,  $176 \pm 8$  K and  $238 \pm 3$  K for the  $\alpha$  process.

According to the theory of Martin, Meier, and Saupe<sup>40</sup>, the splitting of the dynamics to processes  $\alpha$  and  $\delta$  originates from the nematic potential with a magnitude that depends on the nematic order parameter,  $S$ , defined as  $S = \langle (3\cos^2\theta - 1) \rangle / 2$ . The brackets denote a statistical average and  $\theta$  is the angle between the long molecular axis and the preferred direction. According to the theory, the retardation factor,  $g(S)$ , can be obtained from the difference in the time scales of the  $\delta$ - and  $\alpha$ -processes as  $\log(\tau(\delta)/\tau(\alpha)) \sim g(S)$ .<sup>41,42</sup> It has limiting values  $g(S=0)=1$  (isotropic state) and  $g(S \rightarrow 1) \rightarrow \infty$  (fully ordered nematic structure). For  $S < 0.8$ , the following analytic expression has been proposed

$$\log g(S) = 1.069 S + \frac{0.113}{(1-S)^{1.609}} - 0.106 \quad (4)$$

For  $\log(g(S)) \sim 4$  as experimentally observed (Fig. 5), Eq. (4) gives an orientational order parameter with a value of 0.45.

**Table 5: Dielectric strength ( $\Delta\epsilon$ ), permittivity, local field ( $F$ ), and effective dipole moment,  $\mu_{\text{eff}}$ , obtained from DS for molecules **10**, **4** and **5**.**

Samples	$T\Delta\epsilon$ (K)	$\epsilon_s$	$\epsilon_\infty$	$F$	$M$ (g/mol)	$\mu_{\text{eff}}$ (D) <sup>a</sup>
<b>10</b>	174	4.08	3.55	3.58	468.74	1.0
<b>4</b>	2529	12.66	5.68	8.03	518.76	2.6
<b>5</b>	189	4.95	4.45	4.78	799.29	1.2

<sup>a</sup> The density values employed in the calculation of the dipole moments were 1.28, .32 and 1.22 g/cm<sup>3</sup>, respectively for **10**, **4** and **5**.

In conclusion, dicyanobenzothiadiazole molecules can be engineered to engender maximum values of the dipole moment and of the first molecular hyperpolarizability. These properties can be further fine-tuned through the rather small energy barriers of the different conformers. A synthetic strategy is provided by substitution of thiophenes with thiazole or ethenyl-substituents spacers in donor-acceptor polymers, respectively.

This molecular engineering approach has profound effects on the thermodynamic properties, the self-assembly and dynamics. Molecules possessing strong dipole moments crystallize and form spherulitic superstructures whereas molecules with weaker dipoles form liquid crystalline structures. Moreover, all compounds exhibited switchable dielectric permittivity with temperature. In particular compound **4** revealed a large increment in  $\Delta\epsilon$  ( $\sim 11$ ) over a narrow temperature interval that is comparable to the best known rod-like liquid crystals (e.g. comparable to 5-CB<sup>37</sup>). This finding is of particular interest for the design of new solar cells. In this respect, materials processing high dielectric constants are known to improve the charge carrier separation in the photoactive phase<sup>2</sup> or the heterojunction of the donor and the acceptor phase<sup>3</sup>. Lastly, by employing the gas phase dipole moments -the latter obtained

from simulations- allowed calculating the dipole orientation correlation function in the bulk state.

## Conclusion

Based on 4,7-dibromobenzo[c][1,2,5]thiadiazole-5,6-dicarbonitrile (**1**), we synthesized small molecules incorporating thiophene (**3**, **4**, **5**), thiazole (**6**, **7**) and phenyl-acetylene moieties (**8**). Single crystal analysis of the latter showed a reduced steric hindrance. A resulting blue-shifted UV-vis absorption due to lowered donor-strength was observed in **6**, **7** and **8**. However, high fluorescence quantum yields have been observed for all model compounds.

The thienylated derivatives (**3**, **4**, **5** and **9**, **10**, **11**) were investigated with respect to their dipole moments and dipolar dynamics via dielectric spectroscopy with input from DFT calculations. It was shown that these molecules can be engineered to engender maximum values of the dipole moment and of the first molecular hyperpolarizability. A remarkably high dipole moment of DCNBT and of **1**, as compared to BT, has been measured via dielectric spectroscopy. All compounds exhibited switchable dielectric permittivity with temperature. In particular, compound **4** exhibited a large increment in dielectric permittivity ( $\Delta\epsilon \sim 11$ ) over a narrow temperature interval that is comparable to the best known rod-like liquid crystals (e.g. 5-CB).

Although the dielectric permittivity of thienyl derivatives is low at ambient temperature, reflecting the liquid crystalline or crystalline structures - the latter caused by the centrosymmetric crystal unit cell - they are still promising for the design of donor-acceptor copolymers. In D-A copolymers composed of arylenes the absence of crystalline order warrants high dielectric permittivities with values comparable to the ones found in the isotropic phase of the thienyl derivatives (e.g. **4**). An induced orientation of dipolar units at temperatures above the glass temperature, e.g. via corona poling<sup>43,44</sup>, could further enhance the permittivity of donor phases in bulk heterojunction solar cells. This suggests a molecular approach towards decreasing exciton binding energy by “adjusting” the magnitude of dielectric permittivity. This approach, when implemented in OPV, could substantially improve charge carrier separation and increase power conversion efficiency.

## ASSOCIATED CONTENT

The crystal structures of **1** (CCDC: 1533970), **3** (CCDC: 1533733), **4** (CCDC: 1533971), **6** (CCDC: 1533972), **7** (CCDC: 1533973) and **8** (CCDC: 1533734) have been deposited at the Cambridge Crystallographic Data Centre.

## AUTHOR INFORMATION

### Corresponding Author

\* E-mail: muellen@mpip-mainz.mpg.de.

### Present Addresses

†If an author’s address is different than the one given in the affiliation line, this information may be included here.

### Author Contributions

The manuscript was written through contributions of all authors. / All authors have given approval to the final version of the manu-

script. / ‡These authors contributed equally. (match statement to author names with a symbol)

## Funding Sources

This work was financially supported by the Max Planck Society and European Community through the EU Horizon 2020 Research and Innovation Programme under Grant Agreement N. 642196 (iSwitch).

## ACKNOWLEDGMENT

We thank Jutta Schnee for the measurement of fluorescence spectra and Frank Rominger from the institute of organic chemistry in Heidelberg for the measurement of the crystal structure of compound **8**. Patricia Schiel, Tobias Walter and Barbara Gräfen are gratefully acknowledged for the assistance at the synthesis and purification of the compounds. We furthermore thank Dr. Felix Hinkel, Dr. Yulian Zagraniarski and Sebastian Hahn for fruitful discussions. The computations in this paper were run on the Odyssey cluster supported by the FAS Division of Science, Research Computing Group at Harvard University.

## ABBREVIATIONS

## REFERENCES

- de Gier, H.D.; Broer, R.; Havenith, R.W.A. Non-Innocent Side-Chains with Dipole Moments in Organic Solar Cells Improve Charge Separation *Phys. Chem. Chem. Phys.* **2014**, *16*, 12454-12461.
- Cho, N.; Schlenker, C.W.; Knesting, K.M.; Koelsch, P.; Yip, H.-L.; Ginger, D.S.; Jen, A.K.-Y. High-Dielectric Constant Side-Chain Polymers Show Reduced Non-Geminate Recombination in Heterojunction Solar Cells *Adv. Energy Mater.* **2014**, *4*, 1301857.
- Baranovskii, S.D.; Wiemer, M.; Nenashev, A.V.; Jansson, F.; Gebhard, F. Calculating the Efficiency of Exciton Dissociation at the Interface between a Conjugated Polymer and an Electron Acceptor *J. Phys. Chem. Lett.* **2012**, *3*, 1214-1221.
- Abbotto, A.; Seri, M.; Dangate, M. S.; de Angelis, F.; Manfredi, N.; Mosconi, E.; Bolognesi, M.; Ruffo, R.; Salamone, M. M.; Muccini, M. A Vinylene-Linked Benzo[1,2-b:4,5-b']dithiophene-2,1,3-Benzothiadiazole Low-Bandgap Polymer *J. Polym. Sci. A Polym. Chem.* **2012**, *50*, 2829-2840.
- An, C.; Li, M.; Marszalek, T.; Li, D.; Berger, R.; Pisula, W.; Baumgarten, M.; Thiadizoloquinaxaline-Based Low-Bandgap Conjugated Polymers as Ambipolar Semiconductors for Organic Field Effect Transistors *Chem. Mater.* **2014**, *26*, 5923-5929.
- Bundgaard, E.; Krebs, F.C. Low-Band-Gap Conjugated Polymers Based on Thiophene, Benzothiadiazole, and Benzobis(thiadiazole) *Macromolecules* **2006**, *39*, 2823-2831.
- Tsao, H. N.; Cho, D. M.; Park, I.; Hansen, M. R.; Mavrinskiy, A.; Yoon, D. Y.; Graf, R.; Pisula, W.; Spiess, H. W.; Müllen, K. Ultra-high Mobility in Polymer Field-Effect Transistors by Design *J. Am. Chem. Soc.* **2011**, *133*, 2605-2612.
- Yamashita, Y.; Hinkel, F.; Marszalek, T.; Zajaczkowski, W.; Pisula, W.; Baumgarten, M.; Matsui, H.; Müllen, K.; Takeya, J. Mobility Exceeding 10 cm<sup>2</sup>/(V·s) in Donor-Acceptor Polymer Transistors with Band-like Charge Transport *Chem. Mater.* **2016**, *28*, 420-424.
- Kang, I.; Yun, H.-J.; Chung, D. S.; Kwon, S.-K.; Kim, Y.-H. Record High Hole Mobility in Polymer Semiconductors via Side-Chain Engineering *J. Am. Chem. Soc.* **2013**, *135*, 14896-14899.
- Luo, C.; Kyaw, A. K. K.; Perez, L. A.; Patel, S.; Wang, M.; Grimm, B.; Bazan, G. C.; Kramer, E. J.; Heeger, A. J. General Strategy for Self-Assembly of Highly Oriented Nanocrystalline Semiconducting Polymers with High Mobility *ACS Nano Lett.* **2014**, *14*, 2764-2771.

- Zhang, M.; Gu, Y.; Guo, X.; Liu, F.; Zhang, S.; Huo, L.; Russell, T. P.; Hou, J. Efficient Polymer Solar Cells Based on Benzothiadiazole and Alkylphenyl Substituted Benzodithiophene with a Power Conversion Efficiency over 8% *Adv. Mater.* **2013**, *25*, 4944-4949.
- Zhou, H.; Yang, L.; Stuart, A. C.; Price, S. C.; Liu, S.; You, W. Development of Fluorinated Benzothiadiazole as a Structural Unit for a Polymer Solar Cell of 7% Efficiency *Angew. Chem. Int. Ed.* **2011**, *50*, 2995-2998.
- Yang, L. Q.; Tumbleston, J. R.; Zhou, H. X.; Ade, H. You, W. Disentangling the Impact of Side Chains and Fluorine Substituents of Conjugated Donor Polymers on the Performance of Photovoltaic Blends *Energ. Environ. Sci.* **2013**, *6*, 316-326.
- Nielsen, C. B.; White, A. J. P.; McCulloch, I. Effect of Fluorination of 2,1,3-Benzothiadiazole *J. Org. Chem.* **2015**, *80*, 5045-5048.
- Wudarczyk, J.; Papamokos, G.; Margaritis, V.; Schollmeyer, D.; Hinkel, F.; Baumgarten, M.; Floudas, G.; Müllen, K. Hexasubstituted Benzenes Bearing Ultrastrong Dipole Moments *Angew. Chem. Int. Ed.* **2016**, *55*, 3220-3223.
- Lim, J. A.; Lee, W. H.; Lee, H. S.; Lee, J. H.; Park, Y. D.; Cho, K. Self-Organization of Ink-jet-Printed Triisopropylsilyl ethynyl Pentacene via Evaporation-Induced Flows in a Drying Droplet *Adv. Funct. Mater.* **2008**, *18*, 229-234.
- Casey, A.; Han, Y.; Fei, Z.; White, A. J. P.; Anthopoulos, T. D.; Heeney, M. Cyano Substituted Benzothiadiazole: A Novel Acceptor Inducing N-Type Behaviour in Conjugated Polymers *J. Mater. Chem. C* **2015**, *3*, 265-275.
- Tsao, H. N.; Cho, D.; Andreasen, J. W.; Rouhanipour, A.; Breiby, D. W.; Pisula, W.; Müllen, K. The Influence of Morphology on High-Performance Polymer Field-Effect Transistors *Adv. Mater.* **2009**, *21*, 209-212.
- Bronstein, H.; Hurhangee, M.; Fregoso, E. C.; Beatrup, D.; Soon, Y. W.; Huang, Z.; Hadipour, A.; Tuladhar, P. S.; Rossbauer, S.; Sohn, E.-H.; Shoaee, S.; Dimitrov, S. D.; Frost, J. M.; Ashraf, R. S.; Kirchartz, T.; Watkins, S. E.; Song, K.; Anthopoulos, T.; Nelson, J.; Rand B. P.; Durrant, J. R.; McCulloch, I.; Isostructural, Deeper Highest Occupied Molecular Orbital Analogues of Poly(3-hexylthiophene) for High-Open Circuit Voltage Organic Solar Cells *Chem. Mater.* **2013**, *25*, 4239-4249.
- Zaborova, E.; Chavez, P.; Bechara, R.; Leveque, P.; Heiser, T.; Mery, S.; Leclerc, N. Thiazole as a Weak Electron-Donor Unit to Lower the Frontier Orbital Energy Levels of Donor-Acceptor Alternating Conjugated Materials *Chem. Commun.* **2013**, *49*, 9938-9940.
- Gessner, T.; Reichelt, H.; Wudarczyk, J.; Hinkel, F.; Marszalek, T.; Baumgarten, M.; Müllen, K. Preparation of Polymers Comprising at least one Benzo[c][1,2,5]thiadiazol-5,6-dicarbonitrile-Unit. WO 2016/083303.A1, June, 2, **2016**.
- Shi, Q.; Zhang, S.; Zhang, J.; Oswald, V. F.; Amassian, A.; Marder, S. R.; Blakey, S. B.; KOTBu-Initiated Aryl C-H Iodination: A Powerful Tool for the Synthesis of High Electron Affinity Compounds *J. Am. Chem. Soc.* **2016**, *138*, 3946-3949.
- Zhang, J.; Parker, T. C.; Chen, W.; Williams, L.; Khurstalev, V. N.; Jucov, E. V.; Barlow, S.; Timofeeva, T. V.; Marder, S. R. C-H Activated Direct Arylation of Strong Benzothiadiazole and Quinoxaline-Based Electron Acceptors *J. Org. Chem.* **2016**, *81*, 360-370.
- Li, W.; Yan, L.; Zhou, H.; You, W.; A General Approach toward Electron Deficient Triazole Units to Construct Conjugated Polymers for Solar Cells *Chem. Mater.* **2015**, *27*, 6470-6476.
- Dallos, T.; Hamburger, M.; Baumgarten, M.; Thiadiazoloquinoxalines: Tuning Physical Properties through Smart Synthesis *Org. Lett.* **2011**, *13*, 1936-1939.
- Stuart, A. C.; Tumbleston, J. R.; Zhou, H.; Li, W.; Liu, S.; Ade, H.; You, W.; Fluorine Substituents Reduce Charge Recombination and Drive Structure and Morphology Development in Polymer Solar Cells *J. Am. Chem. Soc.* **2013**, *135*, 1806-1815.
- Acharya, R.; Cekli, S.; Zeman, C. J., 4th.; Altamimi, R. M.; Schanze, K. S. Effect of Selenium Substitution on Intersystem Crossing in pi-Conjugated Donor-Acceptor-Donor Chromophores: The LUMO Matters the Most *J. Phys. Chem. Lett.* **2016**, *7*, 693-697.

- <sup>28</sup> Böttcher, C. J. F. Eine Neue Methode zur Berechnung von Dipolmomenten *Rec. Trav. Chim.* **1943**, *62*, 119-133.
- <sup>29</sup> Rizk, H. A.; Elanwar, I. M. Dipole moments of glycerol, isopropyl alcohol, and isobutyl alcohol *Can. J. Chem.* **1968**, *46*, 507.
- <sup>30</sup> Cumper, C.W.N.; Langley, P.G.; Electric Permittivities and Dipole Moments of Solutes in Polar Solvents *Trans. Faraday Soc.*, **1971**, *67*, 35-43.
- <sup>31</sup> Xiao, J.; Zhang, Z.; Wu, D.; Routaboul, L.; Braunstein, P.; Doudin, B.; Losovyj, Y. B.; Kizilkaya, O.; Rosa, L. G.; Borca, C. N.; Gruverman, A.; Dowben, P. A. The Interface Bonding and Orientation of a Quinonoid Zwitterion *Phys. Chem. Chem. Phys.* **2010**, *12*, 10329-10340.
- <sup>32</sup> Cheng, L. T.; Tam, W.; Stevenson, S. H.; Meredith, G. R.; Rikken, G.; Marder, S. R. Experimental investigations of organic molecular nonlinear optical polarizabilities. 1. Methods and results on benzene and stilbene derivatives *J. Phys. Chem.* **1991**, *95*, 10631-10643.
- <sup>33</sup> Kremer, F.; Schönhals, A. *Broadband Dielectric Spectroscopy*, Springer-Verlag, Berlin, Germany, **2002**.
- <sup>34</sup> Floudas, G. *Polymer Science: A Comprehensive Reference*; Matyjaszewski, K. Möller, M., Eds., Elsevier BV, **2012**, Vol. 2.32.
- <sup>35</sup> Haase, N.; Grigoriadis, C.; Butt, H. J.; Müllen, K.; Floudas, G. Effect of Dipole Functionalization on the Thermodynamics and Dynamics of Discotic Liquid Crystals *J. Phys. Chem. B.* **2011**, *115*, 5807-5814.
- <sup>36</sup> Stangenberg, R.; Grigoriadis, C.; Schneider, D.; Butt, H.-J.; Fytas, G.; Müllen, K.; Floudas, G. Self-Assembly Beyond Semifluorinated Alkanes in a Semifluorinated Benzene Derivative *Soft Matter* **2013**, *9*, 11334-11345.
- <sup>37</sup> Stangenberg, R.; Grigoriadis, C.; Butt, H.-J.; Müllen, K. Floudas, G. Switchable Dielectric Permittivity with Temperature and DC-Bias in a Semifluorinated Azobenzene Derivative *Colloid Polym. Sci.* **2014**, *292*, 1939-1948.
- <sup>38</sup> Grigoriadis, C.; Niebel, C.; Ruzié, C.; Geerts Y. H.; Floudas, G. Order, Viscoelastic, and Dielectric Properties of Symmetric and Asymmetric *J. Phys. Chem. B* **2014**, *118*, 1443-1451.
- <sup>39</sup> Ratna, B.R.; Shashidhar, R. Dielectric Properties of 4'-n-Alkyl-4-cyanobiphenyls in their Nematic Phases *Pramana - J. Phys.* **1976**, *6*, 278-283.
- <sup>40</sup> Maier, W.; Meier, G.; Saupe, A. Extended Debye Theory for Dielectric Relaxations in Nematic Liquid Crystals *Faraday Symp. Chem. Soc.* **1971**, *5*, 119-133.
- <sup>41</sup> Seiberle, H.; Stille, W.; Strobl, G. A Comparative Study of Individual and Collective Rotational Motion in Mixtures of Liquid Crystalline Side Group Polymers and Low-Molecular-Weight Mesogens *Macromolecules*, **1990**, *23*, 2008-2016.
- <sup>42</sup> Schönhals, A.; Gessner, U.; Rübner, J. Influence of Lateral Substituents in the Mesogens on the Properties of Liquid-Crystalline Side Group Copolymethacrylates: Dielectric Relaxation Spectroscopy on Homopolymers *Macromol. Chem. Phys.* **1995**, *196*, 1671-1685.
- <sup>43</sup> Dalton, L. R.; Harper, A. W.; Wu, B.; Ghosn, R.; Laquindanum, J.; Liang, Z.; Hubbel, A.; Xu, C. Polymeric Electro-Optic Modulators: Materials Synthesis and Processing *Adv. Mater.* **1995**, *7*, 519-540.
- <sup>44</sup> Hill, R. A.; Knoesen, A.; Mortazavi, M. A. Corona Poling of Nonlinear Polymer Thin Films for Electro-Optic Modulators *Appl. Phys. Lett.* **1994**, *65*, 1733-1735.